AIAA 2000-2371

Radiation Heat Transfer Between Diffuse-Gray Surfaces Using Higher Order Finite Elements

Dana C. Gould
NASA Langley
Hampton, VA

34th AIAA Thermophysics Conference
19-22 June 2000 / Denver, CO

AIAA 2000-2371

RADIATION HEAT TRANSFER BETWEEN DIFFUSE-GRAY SURFACES USING HIGHER ORDER FINITE ELEMENTS

Dana C. Gould

NASA Langley Research Center
Hampton, Virginia 23681-2199

ABSTRACT

This paper presents recent work on developing methods for analyzing radiation heat transfer between diffuse-gray surfaces using *p*-version finite elements. The work was motivated by a thermal analysis of a High Speed Civil Transport (HSCT) wing structure which showed the importance of radiation heat transfer throughout the structure. The analysis also showed that refining the finite element mesh to accurately capture the temperature distribution on the internal structure led to very large meshes with unacceptably long execution times.

Traditional methods for calculating surface-to-surface radiation are based on assumptions that are not appropriate for *p*-version finite elements. Two methods for determining internal radiation heat transfer are developed for one and two-dimensional *p*-version finite elements. In the first method, higher-order elements are divided into a number of sub-elements. Traditional methods are used to determine radiation heat flux along each sub-element and then mapped back to the parent element. In the second method, the radiation heat transfer equations are numerically integrated over the higher-order element. Comparisons with analytical solutions show that the integration scheme is generally more accurate than the sub-element method. Comparison to results from traditional finite elements shows that significant reduction in the number of elements in the mesh is possible using higher-order (*p*-version) finite elements.

INTRODUCTION

Background

One of NASA's main goals is to provide the United States' Aeronautics Industry with the technology it needs to lead the international aerospace industry into the next century. This includes developing enabling technologies, one of which is to "provide next-generation design tools and experimental aircraft to increase design confidence, and cut the development cycle time for aircraft in half."[1] This paper presents initial work on one of these tools, methods for accurate thermal analysis of aircraft structures. The goal of this work is to enable thermal analysis of large-scale components or full aerospace vehicles on a mid-level workstation.

NASA sponsored several projects aimed at reducing barriers to commercially viable high-speed civil and space transportation. The High Speed Research (HSR) Program had a goal "of reducing the travel time to the Far East and Europe by 50 percent within 20 years, and to do so at today's subsonic ticket prices."[1] These aircraft will experience higher in-flight temperatures due to the increased rate of aerodynamic heating associated with high-speed flight. The Reusable Launch Vehicle (RLV) program's goal of "reducing the payload cost to low-Earth orbit by an additional order of magnitude" [1] challenges designers to come up with both materials and structural concepts that can withstand the reentry environment while minimizing the weight of the vehicle. RLV designs are single-stage-to-orbit vehicles that use cryogenic propellant. The propellant tanks are an integral part of the vehicle structure, which, in addition to holding the cryogenic fuel, must withstand the elevated temperatures

Copyright © 2000 by the American Institute of Aeronautics and Astronautics, Inc. No copyright is asserted in the United States under Title 17, U.S. Code. The U.S. Government has a royalty-free license to exercise all rights under the copyright claimed herein for Governmental purposes. All other rights are reserved by the copyright owner.

associated with the reentry. In addition, these materials must also withstand the thermal and structural cycling of repeated flights. Many of the materials that can withstand the elevated temperatures of high-speed flight do not have high thermal conductivity to efficiently dissipate the heat throughout a structure. Thus other modes of heat transfer, radiation in particular, become more significant.[2] The importance of radiation heat transfer as well as the difficulty involved in its modeling was demonstrated by Ko *et al.* [2] in their work on the Space Shuttle thermal analysis. These issues are directly applicable to the design of high-speed commercial aircraft as well as the RLV.

NASA's Space Program also has an interest in improved methodologies for radiation heat transfer. Besides the access to space issue mentioned above, radiation is a dominate mode of heat transfer in most orbiting space structures and satellites. Chin et al. [3] discuss some of the problems associated with thermal modeling of spacecraft, and in particular the problems associated with computation of radiation heat transfer. One of the problems highlighted in reference 3 is the assumption of isothermal, constant radiation heat flux surfaces used in most radiation computations. This assumption tends to under-predict the temperature gradients in the structure. In addition, the assumption of constant radiation heat flux over an element may degrade the accuracy of the calculated temperature field especially where partial shading (blockage) occurs.

The desire for better tools led to an initial study of the heat transfer in a High Speed Civil Transport (HSCT) wing. The study confirmed the significance of radiation in the heat transfer throughout the vehicle's wing structure. The study also demonstrated the relative difficulty of such an analysis, especially when the ultimate goal is to compute the temperatures throughout the whole wing without reverting to reduced models. A summary of this study is given in the following section.

Case Study: High Speed Civil Transport Wing Thermal Analysis

As part of the HSR Program at NASA Langley Research Center (LaRC), a thermal analysis of a HSCT wing was undertaken. The purpose of the analysis was to determine the capabilities of the methods currently used for thermal analysis of aerospace structures and determine what, if any, areas of improvement were required.

The wing geometry model used for the thermal analysis is shown in Figure 1. The wing is approximately 113 feet long at the root and 55 feet wide at the trailing edge. The wing skin was assumed to be constructed of hat-stiffened corrugated panels made from titanium. To model the three-dimensional hat-stiffened skin with two-dimensional elements, equivalent properties (density, capacitance, and thermal conductivity) were derived. For simplicity, this construction was also used for the internal ribs and spars.

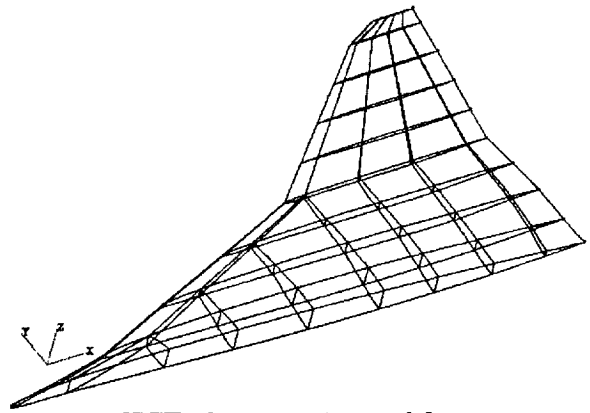

Figure 1: HSCT wing geometry model.

A five-hour flight trajectory, representative of a commercial airline or transport route, was used in the analysis. The majority of the trajectory, 3.8 hours, consisted of a mach 2.4 cruise at an altitude between 60,000 and 70,000 feet. Aerodynamic heating rates were determined using LANMIN, NASA Langley's version of the MINIVER computer code which uses engineering relations to calculate the aerothermal heating (or cooling) to surfaces. The heating rates applied to the upper and lower wing surfaces were generated by MINIVER for each element in the mesh using flat plate boundary layer relations based on the element running length and local flow angle. MINIVER used inviscid flow relations to obtain the undisturbed flow conditions behind the bow shock off the fuselage nose and wing leading edge.

Structural temperatures of the wing throughout the trajectory were computed using MacNeal-Schwendler Corporation's P/Thermal[1] [4] software on a Silicon Graphics Workstation with an R4000 CPU, 96 Mbytes of memory and one Gbyte of disk space. The initial mesh consisted of roughly one element for each geometry surface shown in Figure 1 resulting in 154 nodes and 237 elements. Solutions obtained for this

[1] The use of trademarks or names of manufacturers in this report is for accurate reporting and does not constitute an official endorsement, either expressed or implied, of such products or manufacturers by the National Aeronautics and Space Administration.

mesh both with and without internal radiation showed very little difference in temperature distribution. Note however that all the nodes in this model are located on the wing surfaces (at the intersections of the lines in Figure 1) where the heat transfer is dominated by the aerodynamic heating. Thus all the computed temperatures respond very quickly to changes in the aerodynamic heating rates. The lack of nodes along the internal structure, where temperatures are not directly affected by the aerodynamic heating and thus respond slower, results in a misleading temperature distribution for the wing structure.

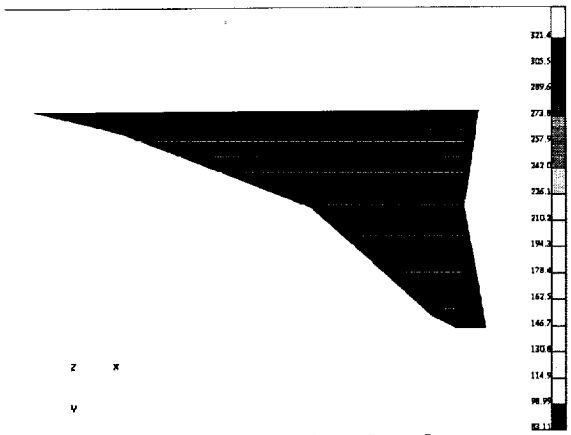

Figure 2: HSCT wing, refined mesh and temperature contours (Temperatures in °F).

A second analysis was performed with a mesh refined to have elements with edge lengths of 18 inches on both the internal structure and wing surfaces. This mesh size was driven by the desire to have at least two elements across the height of the internal structure while keeping the overall size of the model within reason. The mesh, which consisted of 3624 nodes and 4037 elements, is shown in Figure 2 overlaid on a contour plot of the lower surface temperature at the beginning of cruise. The solution shown in Figure 2 did not include internal radiation heat transfer because the view factor calculation never ran to completion. It is also interesting to note that the view factor computation required over 600 Mbytes of disk space before crashing! Neglecting internal radiation resulted in a peak internal temperature of less than 150°F and a temperature gradient of 220°F across the internal structure at the beginning of cruise. The large temperature difference between the external and internal structures raises the possibility of significant radiation exchange.

The problems with the view factor calculation as well as the desire to get a more detailed temperature distribution for the internal structure led to the development of a wing box model. This model allowed for a more detailed analysis of a smaller section of the wing, in this case a box defined by adjacent ribs and spars and the corresponding upper and lower surface sections. Solid elements with equivalent properties were used for all sides of the box so that temperature gradients through the thickness of the panels could be determined in addition to the effects of internal radiation. The finite element mesh used for the wing box thermal analysis is shown in Figure 3.

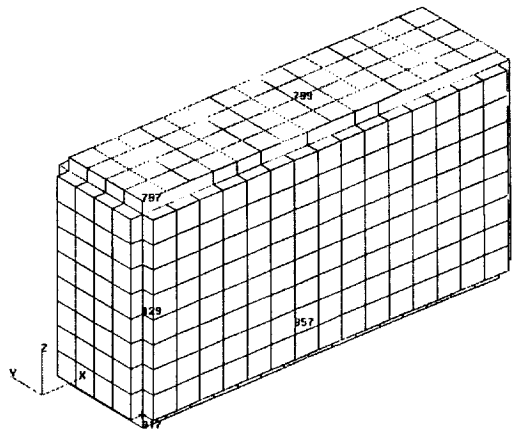

Figure 3: Finite element mesh used for the thermal analysis of a wing box (Note node 957 is located on the lower wing surface).

The model was first run without internal radiation and the transient temperature response of the nodes labeled in Figure 3 are shown in Figure 4. Internal radiation was added for the next run and the results are shown in Figure 5. These figures clearly show the significant impact of internal radiation heat transfer on the temperatures of the internal wing structure. Ko *et al.* have also shown the importance of internal radiation in their work on the Space Shuttle[2]. Their results for the in-plane temperature distributions for the upper and lower surfaces suggest that higher order basis functions might be well suited to this application. This behavior coupled with the difficulties encountered using traditional methods lead to the idea of applying hierarchical *p*-version elements to radiation heat transfer in enclosures.

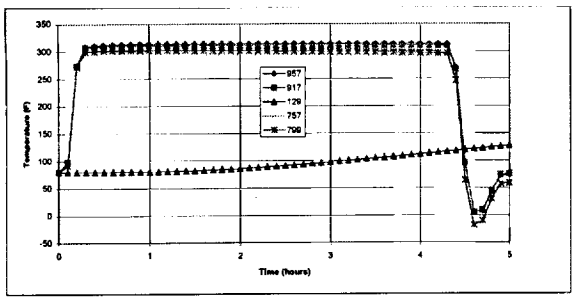

Figure 4: Transient temperatures for wing box model with no internal radiation.

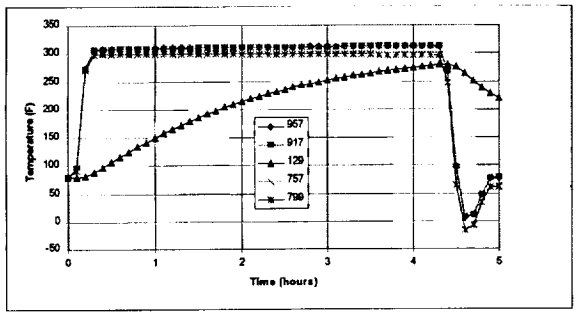

Figure 5: Transient temperatures for wing box model with internal radiation.

FINITE ELEMENT FORMULATION

The finite element method and its application to thermal problems is well established. For the interested reader, Huebner *et al.* [5] provides a detailed formulation of the problem. Here it will simply be noted that the approach begins by subdividing the problem region into elements and approximating the temperature in each element with some function in the form of

$$T^{(e)}(x,y,z,t) = \sum_{i=1}^{r} N_i(x,y,z)T_i(t) \qquad (1)$$

where N_i are interpolation functions and T_i nodal quantities related to the temperature at time t. The corresponding finite element equations can be written (see [5]):

$$[C]\left\{\frac{dT}{dt}\right\} + [[K_c] + [K_h]]\{T\} = \{R_Q\} + \{R_q\} + \{R_h\} + \{R_r\} \qquad (2)$$

where

$$[C] = \int_{\Omega^{(e)}} \rho c_p \{N\}[N]\, d\Omega$$

$$[K_c] = \int_{\Omega^{(e)}} [B]^T [k][B]\, d\Omega$$

$$[K_h] = \int_{\partial\Omega^{(e)} \cap S_2} h\{N\}[N]\, d\Gamma$$

$$\{R_Q\} = \int_{\Omega^{(e)}} Q\{N\}\, d\Omega$$

$$\{R_q\} = \int_{\partial\Omega^{(e)} \cap S_1} q_s\{N\}\, d\Gamma$$

$$\{R_h\} = \int_{\partial\Omega^{(e)} \cap S_2} hT_f\{N\}\, d\Gamma$$

$$\{R_r\} = -\int_{\partial\Omega^{(e)} \cap S_3} q_r\{N\}\, d\Gamma$$

$$[B] = \begin{bmatrix} \frac{\partial N_1}{\partial x} & \frac{\partial N_2}{\partial x} & \cdots & \frac{\partial N_r}{\partial x} \\ \frac{\partial N_1}{\partial y} & \frac{\partial N_2}{\partial y} & \cdots & \frac{\partial N_r}{\partial y} \\ \frac{\partial N_1}{\partial z} & \frac{\partial N_2}{\partial z} & \cdots & \frac{\partial N_r}{\partial z} \end{bmatrix}$$

with r, c_p, and k being the material density, specific heat, and thermal conductivity, respectively. Boundary conditions included in the above definitions are: specified heat flux q_s on surface S_1, convection on surface S_2 with a convection coefficient h and a fluid temperature T_f, and net radiation heat flux q_r on surface S_3. Q represents any heat source or sink in the material.

In general, any given element in the solution domain will not have all of the above terms. For example, only elements on the surface of the domain will have the terms associated with the boundary conditions, and even then they will only have the terms associated with the boundary conditions that apply to the element. The terms are calculated individually for each element in the domain and then assembled into a global system of equations using traditional finite element techniques [5].

Traditional methods for determining the radiation heat transfer flux q_r are based on the assumptions that surfaces are isothermal and the incident radiant heat fluxes on them are uniform. The isothermal surface assumption is inconsistent with finite-element formulation since the temperature over the element varies according to its shape function. To minimize the error introduced by this assumption, the mesh size must be controlled to limit the temperature variation over an element surface. This can lead to a large number of elements for structures with large temperature variation throughout. View factors will have to be computed between all of these surfaces, a process that requires N^2 computations for N elements. Also, since radiation links surfaces throughout a structure, matrices are no longer sparse as they are with conduction problems. Thus mesh refinement in a radiation heat transfer problem can quickly become overwhelming as demonstrated in the case study. In addition, Lobo and

Emery [6] report that with intense radiation heat fluxes, methods employing low-order basis functions can produce erroneous results.

An alternative to mesh refinement (*h*-refinement) is to increase the order of the basis functions in the finite-element formulation (*p*-refinement). In a follow-up report to their earlier work (cited above), Lobo and Emery [7] demonstrate that the errors occurring under intense radiation heat flux conditions are due to the violation of the Discrete Maximum Principle. They show that one way to alleviate this problem is to use higher-order basis functions along the surfaces of radiating elements. Surana *et al.*[8] have demonstrated the effectiveness of *p*-version finite element methods for conduction problems, but they do not include radiation. Kuppurao and Derby [9] use linear and quadratic basis functions for pure radiation problems arising in crystal growth systems, and develop several methods which do not rely upon the isothermal assumption. This work takes a slightly different approach to implementing higher-order basis functions and presents results for test problems representative of the wing box analysis.

RADIATION HEAT TRANSFER WITH HIGHER ORDER ELEMENTS

Fundamental to the accurate implementation of the *p*-method in heat transfer problems with enclosure radiation is the accurate computation of the radiant heat flux q_r, and it's variation, over a surface. The governing equations for the radiant heat flux are of integral form. By assuming the surfaces are isothermal with uniform radiant heat fluxes, these integral equations can be separated into a set of integral geometry equations (view factors) and net radiation equations (algebraic set of equations). Forgoing these assumptions leaves a set of simultaneous integral equations that must be solved. Daurelle et al. [10, 11] shows that solving the set of integral equations leads to more accurate results even when using linear basis functions for the temperature field. Their work indicates that the set of integral equations is slower to solve for a given mesh; however, for a given accuracy the set of integral equations is twice as fast as the traditional approach using the isothermal surface with uniform radiant heat flux assumptions. Two methods are developed here: the Radiation Sub-Element method, which takes advantage of the well-developed traditional methods; and the more accurate Integration method, which solves a set of integral equations.

Radiation Sub-Elements (RSE)

The Radiation Sub-Element approach is the simplest and most straightforward technique to implement variable surface radiation. Any code that can currently handle surface-to-surface radiation can implement this procedure without major modifications. This approach breaks the radiation elements into sub-elements for the surface to surface radiation exchange problem. These radiation sub-elements are then treated in the classical approach, i.e. assume that they are isothermal and then calculate view factors and absorbed heat fluxes. The sub-element absorbed heat fluxes are then transferred back to the parent element generating a variable radiation heat flux along the element. Several different methods to approximate the varying heat load on the element have been investigated.

A one-dimensional problem was used to determine how accurately the absorbed heat flux should be modeled. The energy equation for one-dimensional heat conduction in a rod with an applied heat flux q^p is:

$$kA\frac{d^2T}{dx^2} = q^p(x)S$$

where

k is the thermal conductivity, A is the cross sectional area of the rod, S is the rod's surface area, and q^p is the variable heat flux expressed as a polynomial in x. Integrating twice gives the general solution:

$$T(x) = \frac{S}{kA}\iint q^p(x)dxdx + c_1x + c_2$$

The point of interest here is that the temperature solution is a polynomial of order $p + 2$, that is, it is 2 orders higher than the polynomial describing q. Applying this to finite element analysis, given a shape function of order m for the temperature distribution along a rod element, the radiation heat flux should be calculated to an order of $m - 2$.

Five methods to transform the discrete heat fluxes on the radiation sub-elements to a continuous function on their parent element were investigated. Two two-dimensional test problems with one-dimensional elements were solved using sixth order polynomials for temperature interpolation function on the elements. The radiation load vectors were calculated to fourth order. This required dividing each element into five radiation sub-elements yielding five absorbed heat fluxes for each parent element. These five heat fluxes were then integrated (numerically) with the shape functions to generate the radiation load vector $\{R_r\}$ in equation 2.

The first method models the heat flux along the element as a step function. This is consistent with the method used for generating the heat fluxes (the classical approach assumes the incident radiation to be constant along a surface). However, incident radiation does not typically vary in this fashion, rather it is usually a smooth function which may have significant variation depending on the geometry involved. (And if higher order elements are being used for the analysis, there probably are large variations along the element.)

The second method approximated the heat flux by linearly interpolating between the five heat flux values. The heat fluxes were placed at their sub-element centroid for the interpolation process. This method interpolates between two values when possible, otherwise the closest value is used. Values outside of two element centroids (i.e., near the open ends of the surface) are assigned the same value as the element centroid.

A simple extension of the interpolation method is the interpolation/extrapolation method. As the name implies, this method simply extrapolates the local heat flux value when interpolation is not possible. While this method may lead to more accurate solutions in many problems, it may also lead to problems if the extrapolated values become unrealistic.

To improve the absorbed radiation heat flux approximation a fourth order curve fit was implemented next. The five heat fluxes were located at their sub-element centroid, and a fourth order polynomial was fit to the points.

The final radiation heat flux approach uses cubic splines. Once again the question arises as to how to best extrapolate the data when interpolation is not possible (i.e. near the end points of an element). Three extrapolation methods for the cubic spline were investigated. The first approach, also called a natural cubic spline, sets the second derivative of the curve to zero at the end points. This translates to a linear extrapolation of the heat flux values and yielded the poorest results. The second method extrapolated the data based on a constant second derivative. This significantly improved the results. The third method allows for a fully cubic curve at the end points and is based on a linearly extrapolated second derivative. This proved to be the most accurate of all the RSE methods, and while no problems were encountered in testing, it still extrapolates data and therefore is susceptible to the problems associated with such operations.

Integration Method (IM)

Regardless of the approach used in the RSE method to approximate the radiation heat flux on an element, the approximation is based on data from the traditional calculation procedures. While this makes implementation simple, it still suffers from the assumptions used in developing the traditional approaches, namely the uniform temperature and uniform incident radiation assumptions (albeit they are made on sub-elements).

To study the problem without making the above assumptions consider an element k that is part of an enclosure of N elements. A heat balance at the point x_k on element k is:

$$q_k(x_k) = H_k(x_k) - J_k(x_k) \tag{3}$$

where

$$H_k(x_k) = \varepsilon_k \sigma T_k^4(x_k) + \rho_k J_k(x_k) \tag{4}$$

$$dA_k J_k(x_k) = \sum_{j=1}^{N} \int_{A_j} H_j(x_j) dF_{dj-dk}(x_j, x_k) dA_j$$

This last equation can be simplified by applying the reciprocity relation

$$dA_j dF_{dj-dk} = dA_k dF_{dk-dj}$$

to give

$$J_k(x_k) = \sum_{j=1}^{N} \int_{A_j} H_j(x_j) dF_{dk-dj}(x_j, x_k)$$

Substituting this expression into equation 3 gives:

$$q_k(x_k) = H_k(x_k) - \sum_{j=1}^{N} \int_{A_j} H_j(x_j) dF_{dk-dj}(x_j, x_k) \tag{5}$$

Equations 3 and 4 can be combined to eliminate the surface irradiation term yielding:

$$H_k(x_k) = \sigma T_k^4(x_k) - \frac{1-\varepsilon_k}{\varepsilon_k} q_k(x_k)$$

which can then be substituted back into equation 5 for H_k and H_j (with the subscript changed from k to j) to give

$$\frac{q_k(x_k)}{\varepsilon_k} = \sigma T_k^4(x_k) - \sum_{j=1}^{N} \int_{A_j} \left[\sigma T_j^4(x_j) - \frac{1-\varepsilon_j}{\varepsilon_j} q_j(x_j)\right] dF_{dk-dj}(x_j, x_k) \tag{6}$$

This equation relates the net surface heat flux to the surface temperatures. Note that it is a nonlinear integral

equation and that to calculate the heat flux on surface k, the surface heat flux on all other surfaces must be known in addition to the temperatures of all surfaces (including surface k). While this might seem a bit more complex, recall that an iterative solution technique is generally required to solve the nonlinear finite element equations. Thus, the temperatures and heat fluxes from the previous iteration values can be used on the right hand side of equation 6.

There are several ways to evaluate equation 6, but doing it numerically will only give a single value at some point x_k. Thus to obtain a function $q_k(x_k)$, some approximation method similar to those shown in the RSE method is required. But the radiation heat flux is only used to calculate a load vector $\{R_r\}$, where it is multiplied by the element shape function and integrated over the area of the element. If this integration is done numerically, the heat flux does not need to be a continuous function; it only needs to be evaluated at the points defined by the numerical integration scheme.

The approach taken here is to evaluate the radiation load vectors using Gauss Integration. Thus the heat flux on an element only need be determined at the Gauss points along the element. Also, by using the same integration scheme to evaluate the integrals in equation 6, no approximating function $q_k(x_k)$ is required. The following steps are used to determine the radiation load vector for this solution method:

1. Initialize unknowns (temperatures and radiation heat fluxes).
2. Calculate differential form factors between Gauss points on all elements.

(Begin iteration)

3. Calculate radiation heat fluxes at Gauss points on all elements.
4. Integrate radiation heat fluxes to obtain radiation heating load vector.
5. Solve for and update temperatures.
6. Check convergence and repeat iteration if necessary (go to step 3).

APPLICATION

Two-Dimensional Test Problems

To investigate these techniques, two simple test problems were developed. The test problems involve two one-dimensional elements in radiative equilibrium. The first test problem, shown in Figure 6, represents heat transfer in the corner of a rectangular enclosure. The two elements are oriented at right angles with each other and share a common end point location (there is a separate node at this location for each element). The vertical element is held at a constant temperature of 1000°R and the horizontal element is allowed to come to radiative equilibrium. The horizontal element's length was set to 5 times the vertical element length in order to allow a reasonable temperature gradient to develop along the element. Both surfaces were modeled as black bodies so that an exact solution could be found.

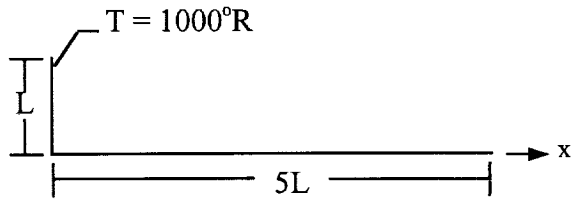

Figure 6: Schematic of test problem 1.

The second test problem is shown in Figure 7. This problem considers two parallel black plates each of length L separated a distance d apart. Once again the top plate was held at a constant temperature and the other plate allowed to come to radiative equilibrium. Results presented here are for a d/L ratio of 0.1.

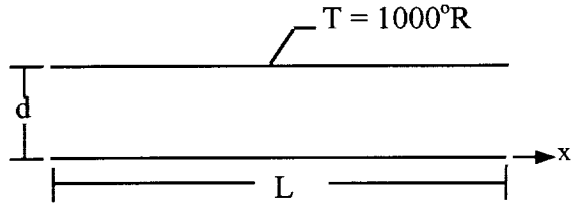

Figure 7: Schematic of test problem 2.

Results

Radiation Sub-element Method

Results for test problem 1 using the RSE methods are shown in Figure 8. Results for all the methods of approximating the radiation heat loads are shown along with the exact solution. Although the step function method is consistent with the isothermal/uniform heat flux assumption used to generate the heat flux data, the resulting temperature prediction was poor with the error approaching 20% at the element end points.

Results of the interpolation method are slightly better than the step function results; however, both methods significantly under-predict the peak temperature at x/L = 0. The problem here is that the incident heat flux is rising rapidly (x/L = 0 corresponds to the corner location). Both the step function and linear interpolation methods model the heat flux as constant in

this area (step function holds the value constant from x/L = 0 to 0.2, linear interpolation function holds the value constant from x/L = 0 to 0.1) and thus under-predict the actual temperature. Extrapolating the data near the endpoints improves the results considerably cutting the error at these locations by approximately 50%. The extrapolated heat flux values still under predict the actual heat flux values near x/L=0, and over predict the actual heat flux values near x/L=5.

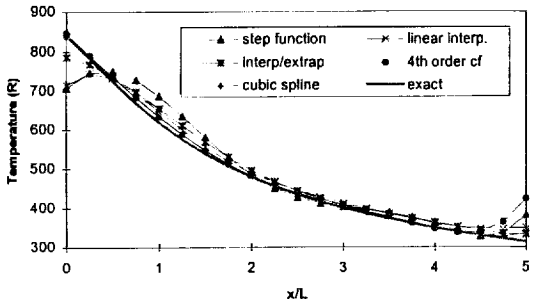

Figure 8: Results for test problem 1.

The fourth order curve fit gives excellent results over most of the element; however, there is a significant error in the temperature at x/L of 5. This behavior is due to the nature of the fourth order polynomial defined by the 5 heat flux values. While the actual radiation heat flux for this problem continues to decrease slowly as x/L approaches 5, the polynomial fit begins to increase here. Several approaches could be implemented to avoid this problem; however, while extrapolating the results is causing errors at x/L=5, it is helping yield a better answer at x/L=0. One approach that would certainly improve the results for this case would be to subdivide the element into additional radiation sub-elements and use a curve fit to smooth out the polynomial. The problem here is the additional computations required for the new sub-elements.

Finally, the cubic spline curve fit gave the best overall results. The results shown in Figure 8 are for the fully cubic spline. The temperature results show good agreement over the whole element with the largest errors occurring near x/L=5.

In general all the approximation methods suffer near the endpoints, regions where the data must be extrapolated. These methods may be improved by calculating the heat flux at the endpoints of the element. This would require computation of radiation heat fluxes at points, as opposed to finite surfaces. The traditional methods used to calculate the heat fluxes on an element would have to be modified to handle both finite areas as well as points; however, this complication is only minor and may well be worth the additional effort. Another consequence which might prove more significant is that the interior points would be farther apart (assuming only 5 points) possibly increasing the approximation error in the interior of the element.

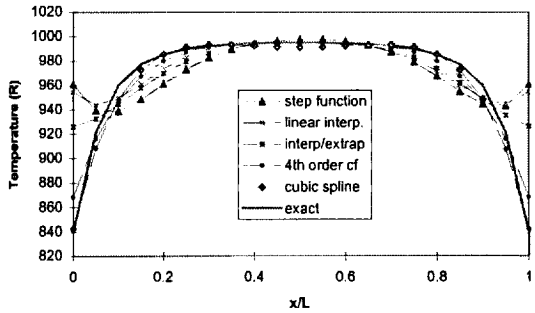

Figure 9: Results for test problem 2.

Figure 9 shows the results of these methods applied to test problem 2 along with the exact solution. The results are similar to those from test problem 1 with the cubic spline curve fit method giving the best overall results. To quantify the overall performance of the various methods, the following error indicator was calculated for each method:

$$error\ indicator = \sqrt{\frac{\sum_i \left(T_{FE} - T_{exact}\right)^2}{\sum T_{exact}^{\ 2}}}$$

where T_{FE} is the temperature from finite element calculation, T_{exact} is the temperature from the analytical solution, and i indicates the number of the i^{th} data point shown in the figures (total of 21points)

This error indicator is shown in Figure10 for test problem 1 and in Figure 11 for test problem 2. As expected the cubic spline curve fit has the lowest error indicator value.

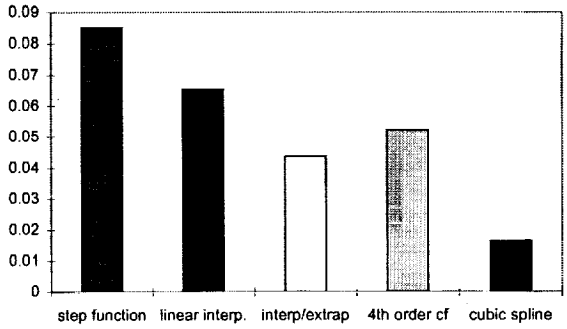

Figure 10: Error indicator for test problem 1.

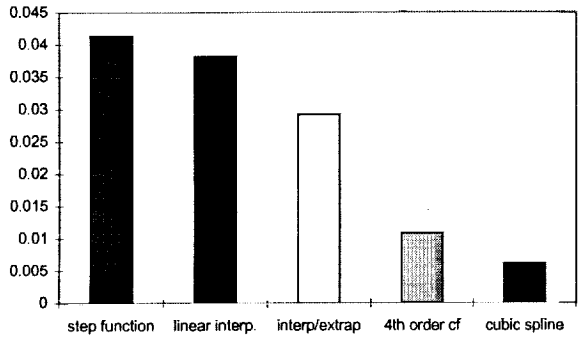

Figure 11:Error indicator for test problem 2.

Integration Method

The results for test problem 1 using the integration method are shown in Figure 12. The figure shows results using a 7 Gauss point integration scheme, which performs so well that it is difficult to distinguish between the integration method and the exact solution. The results for the cubic spline radiation sub-element method are also included to gage how well the integration method performs against the best radiation sub-element method. The integration method has nearly an order of magnitude reduction in the error indicator.

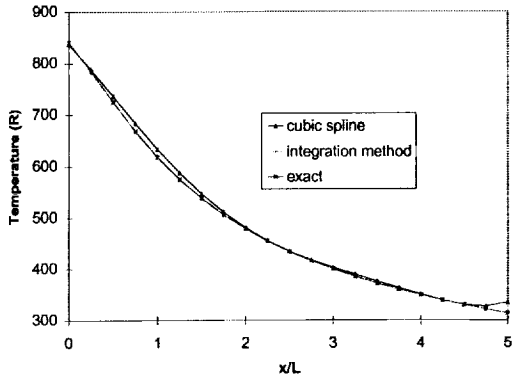

Figure 12: IM vs. RSE results for test problem 1.

Results for test problem 2 are shown in Figure 13. Once again results for the cubic spine radiation sub-element method are included for comparison. Note that the integration method slightly over-predicts the temperature at the center of the element while the radiation sub-element method slightly under-predicts the temperature there. The integration method used 16 Gauss points to obtain this solution, significantly more than was necessary for the first test problem. This higher accuracy scheme was necessary because of the geometry associated with test problem 2, namely large surfaces separated by a small distance. This is a common problem in radiation heat transfer and view factor calculations and is discussed in many view factor references.

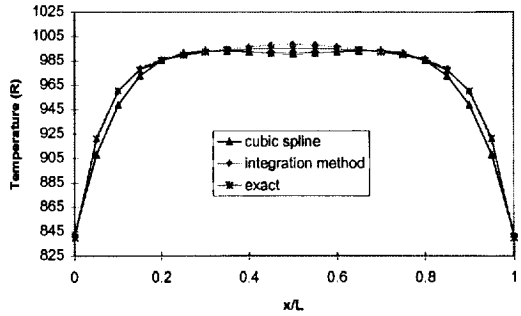

Figure 13: IM vs. RSE results fro test problem 2.

Several additional finite element analyses were performed to compare these methods to traditional methods for computing radiation heat transfer. Each test problem was analyzed using the traditional finite element approach–linear shape functions for the temperature field with the radiation heat flux assumed constant over each element. Each surface was subdivided into a number of linear elements and the mesh was refined until the error indicator was reduced to the level produced by the higher-order methods. Table 1 lists the number of linear elements required to match the solution accuracy of the new methods. The traditional approach required 10 elements for test problem 1 and 17 elements for test problem 2 to match the error indicator for a single element using the cubic spline radiation sub-element method. Similarly, the traditional approach required 46 elements for test problem 1 and 42 elements for test problem 2 to match the error indicator for a single element using the integration method. These traditional analyses were carried out using a totally separate computer code previously developed by the author. This code had very little similarity to the code used to develop the higher order methods, so no attempt was made to compare the computational costs (run times) for the methods.

Table 1: Number of linear elements required to match the accuracy of a single p = 6 element using the RSE and IM methods.

Test problem	Radiation sub-element method (cubic spline curve fit)	Integration method
1	10	46
2	17	42

Three-Dimensional Test Problem

Based on the results from the two-dimensional test problems, the cubic spline curve fit RSE and integration methods were implemented in a three-dimensional finite element code. The test problem for this case, shown in Figure 14, consists of two parallel six-inch square plates separated by a distance of six inches. The top plate is held at 1000°F and there is no conduction in either plate. The emissivity of both plates is 1.0 so that the analytical solution could be obtained:

$$T(x,y) = 1000\left[\int_0^6\int_0^6 \frac{36}{\pi\left[(x-\bar{x})^2+(y-\bar{y})^2+36\right]^2}\,d\bar{x}\,d\bar{y}\right]^{\frac{1}{4}}$$

A surface plot of this solution is shown in Figure 15.

A slightly different method was used to measure the accuracy of the solutions for this test problem so that comparison with *h*-refinement could be made. The L^2 norm of the error for element K is:

$$\|e\|^2_{L^2(K)} = \int_K (T_{analytic} - T_{finite\ element})^2\,dx\,dy$$

The error for the problem is found by taking the square root of the sum of all the element errors in the domain Ω:

$$\|e\|^2_{L^2(\Omega)} = \sqrt{\sum_K \|e\|^2_{L^2(K)}}$$

Solutions for this problem were generated using *h*-refinement with the traditional radiation approach (isothermal surfaces with uniform radiation heat flux); L^2 norms for these cases are shown in Table 2. The amount of mesh refinement was limited by limitations in the view factor software; however, the cases presented give a good indication of how quickly the error drops with *h*-refinement. Results for the radiation sub-element method are presented in Table 3. The data indicate that increasing the interpolation function gives more accurate solutions for a given number of degrees of freedom. However, the integration method provides the best accuracy as the data in Table 4 show. Only the even polynomial results are presented because the solution is an even function, and the odd polynomials do not improve the solution accuracy. Note that using a single element with a polynomial of order 2 (in each direction) with the integration method provides a solution more accurate than any of the other approaches. For nine degrees of freedom, the *h*-refinement L^2 error norm is 19.45, the radiation sub-element method with nine degrees of freedom has an L^2 error norm of 1.97 and the integration method with nine degrees of freedom has an L^2 error norm of 0.23. In all cases, for a given number of degrees of freedom, the integration method produces the lowest error followed by the radiation sub-element method with the *h*-refinement method giving the largest error.

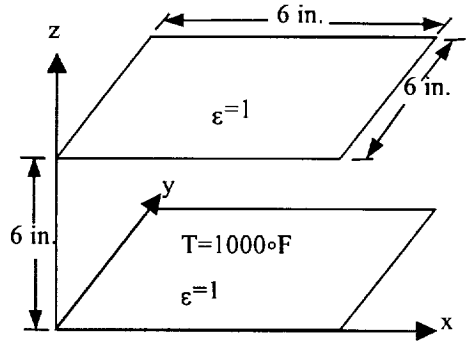

Figure 14: Parallel plates under radiation equilibrium conditions with the lower plate held at a uniform temperature.

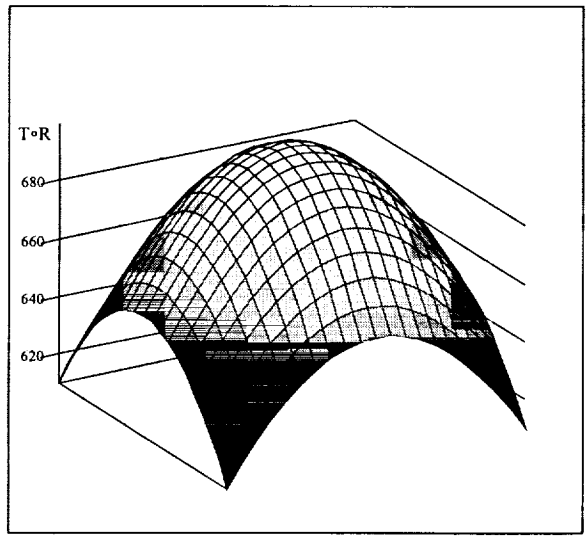

Figure 15: Analytical solution for 3-D test problem.

Table 2: Error norms for h-refinement using the traditional radiation method.

Number of p=1 elements	Number of degrees of freedom	L^2 error norm
1	4	19.4522
4	9	19.4522
9	16	9.74385
16	25	6.51942
25	36	4.65848
36	49	3.56349
49	64	2.83546
64	81	2.32688
81	100	1.95422
100	121	1.67149
400	441	0.59645

Table 3: Error norms for *p*-refinement using the radiation sub-element method.

Order of element (p)	Number of degrees of freedom	L^2 error norm
1	4	19.4522
2	9	1.96614
3	16	1.10128
4	25	0.73404
5	36	0.52810
6	49	0.40612

Table 4: Error norms for *p*-refinement using the integration method.

Order of element (p)	Number of degrees Of freedom	L^2 error norm
1	4	19.4547
2	9	0.23185
4	25	0.00789
6	49	0.00081

CONCLUSIONS

Two methods for determining internal radiation heat transfer have been developed for higher-order finite elements. The first method divides the higher-order element into a number of sub-elements, calculates the radiant heat flux on the sub-elements using traditional methods, and then curve fits this data to determine the radiation heat flux along the higher-order parent element. The second method numerically integrates the radiation heat transfer equations over the higher-order element using an efficient Gaussian integration scheme. Comparisons with analytical solutions show that the integration scheme is generally more accurate than the sub-element method. Comparisons of these results to those of traditional linear finite elements demonstrate the potential for improved computational performance given a required level of accuracy.

References

1. Aeronautics & Space Transportation Technology: Three Pillars for Success, Office of Aeronautics & Space Transportation Technology, National Aeronautics and Space Administration, Washington, D.C., March 1997

2. Ko, W. L., Quinn, R. D., Gong, L., *Finite-Element Reentry Heat-Transfer Analysis of Space Shuttle Orbiter*, NASA T.P. 2657, 1986.

3. Chin, J. H., Panczak, T. D., Fried, L., "Spacecraft Thermal Modelling", *International Journal for Numerical Methods in Engineering*, Vol. 35, No. 4, 1992.

4. MSC/PATRAN User Manual, MacNeal-Schwendler Corporation, Version 6.0 (August 1996).

5 . Huebner, K. H., Thornton, E. A., Byrom, T. G., *The Finite Element Method for Engineers*, 3rd ed., John Wiley and Sons, New York, 1995.

6. Lobo, M., Emery, A. F., "Special Radiation Elements and Their Interfacing for Thermal Radiation Analysis", *Radiation Heat Transfer*, ASME HTD Vol. 154, 1990, pp. 1-8.

7. Lobo, M., Emery, A. F., "The Discrete Maximum Principle in Finite-Element Thermal Radiation Analysis", *Numerical Heat Transfer, Part B: Fundamentals*, Vol. 24, 1993, pp. 209-227.

8. Surana, K. S., Teong, K. W., "p-Version Three Dimensional Solid Element for Heat Conduction", *Mechanics Computing in 1990's and Beyond*, Proceedings of the Conference, ASCE, New York, NY, 1991, pp. 142-146.

9. Kuppurao, S., Derby, J. J., "Finite-Element Formulations for Accurate Calculation of Radian Heat Transfer in Diffuse-Gray Enclosures", *Numerical Heat Transfer, Part B: Fundamentals*, Vol. 24, 1993, pp. 431-454.

10. Daurelle, J. V., Occelli, R., Martin, R., "Finite-Element Modeling of Radiation Heat Transfer Coupled with Conduction in an Adaptive Method", *Numerical Heat Transfer, Part B: Fundamentals*, Vol 25, 1994, pp. 61-73.

11. Daurelle, J. V., Occelli, R., Martin, R., "Modelization by Finite Element Analysis of Radiative Heat Transfers with Non Constant Radiative Properties Coupling with Conduction", *Advanced Computational Methods in Heat Transfer II, Vol. I: Conduction, Radiation and Phase Change*, Computational Mechanics Inc. Billerica, MA,1992, pp. 195-204.